PCCP

Thermodynamic aspect of sulfur, polysulfide anion and lithium polysulfide: Plausible reaction path during discharge of lithium-sulfur battery

Thermodynamic aspect of sulfur, polysulfide anion and lithium polysulfide: Plausible reaction path during discharge of lithium-sulfur battery

Seiji Tsuzuki,[a*] Tomoaki Kaneko,[b] Keitaro Sodeyama,[b] Yasuhiro Umebayashi,[c] Wataru Shinoda,[d] Shiro Seki,[e] Kazuhide Ueno,[f] Kaoru Dokko,[fg] Masayoshi Watanabe[f]

[a] Research Center for Computational Design of Advanced Functional Materials (CD-FMat), National Institute of Advanced Industrial Science and Technology (AIST), 1-1-1 Umezono, Tsukuba, Ibaraki 305-8568, Japan. E-mail: s.tsuzuki@aist.go.jp

[b] Research and Services Division of Materials Data and Integrated System, National Institute for Materials Science (NIMS), 1-1 Namiki, Tsukuba, Ibaraki 305-0044, Japan.

[c] Graduate School of Science and Technology Niigata University 8050, Ikarashi, 2-no-cho, Nishi-ku, Niigata 950-2181, Japan

[d] Department of Materials Chemistry, Nagoya University, Furo-cho, Chikusa-ku, Nagoya 464-8603, Japan

[e] Department of Environmental Chemistry and Chemical Engineering, School of Advanced Engineering, Kogakuin University, 2665-1 Nakano-machi, Hachioji, Tokyo 192-0015, Japan

[f] Department of Chemistry and Biotechnology, Yokohama National University, 79-5 Tokiwadai, Hodogaya-ku, Yokohama 240-8501, Japan

[g] Unit of Elements Strategy Initiative for Catalysts & Batteries (ESICB), Kyoto University, Kyoto 615-8510, Japan

Abstract

Elucidation of elemental redox reactions of sulfur is important for improving the performance of lithium-sulfur batteries. The energies of stable structures of S_n, $S_n^{\cdot-}$, S_n^{2-}, $[LiS_n]^-$ and Li_2S_n (n = 1-8) were calculated at the CCSD(T)/cc-pVDZ//MP3/cc-pVDZ level. The heats of reduction reactions of S_8 and Li_2S_n with Li in solid phase were estimated from the calculated energies and sublimation energies. The estimated heats of redox reactions show that there are several redox reactions with nearly identical heats of reactions, suggesting that several reactions can proceed simultaneously at the same discharge voltage, although the discharging process was often explained by stepwise reduction reactions. The reduction reactions for the formation of Li_2S_n (n = 2-6 and 8) from S_8 normalized as one electron reaction is more exothermic than that for the formation of Li_2S directly from S_8, while the reduction reactions for the formation of Li_2S from Li_2S_n are slightly less exothermic than that for the formation of Li_2S directly from S_8. This suggests that a two-step discharge curve, where the reduction reactions for the formation of Li_2S_n (n = 2-6 and 8) from S_8 occur first, followed by the formation of Li_2S, is observed, if reduction reactions with large heat generation are favored.

Introduction

Lithium-sulfur batteries have been considered promising next-generation secondary batteries owing to their high energy density and low cost.[1-3] Theoretical energy density of lithium-sulfur batteries (2567 Whkg^{-1}) is more than five times greater than that of lithium ion batteries (387 Whkg^{-1} for $LiCoO_2$/C).[4,5] Lithium-sulfur batteries have been actively studied for the last decade.[4,6-12] The dissolution of Li_2S_n, which are generated by the reduction of sulfur, in the electrolytes of lithium-sulfur batteries is a problem for improving the performance of lithium-sulfur batteries. Recently several electrolytes in which Li_2S_n is insoluble and all-solid-state lithium-sulfur batteries were studied to avoid the problem.[13,14] Understanding the mechanism of Li_2S formation in discharging process in lithium-sulfur batteries using such electrolyte that does not dissolve Li_2S_n is essential for improving the performance of lithium-sulfur batteries.[15-19] When discharging, S_8 reacts with Li to form Li_2S. The discharging process was often explained by stepwise reduction reactions such as S_8 -> Li_2S_4 -> Li_2S_2 -> Li_2S.[5,8,9,20,21] But various lithium polysulfides (Li_2S_n, n=2-8) can be produced during the discharging process. It has been pointed out that the intermediate Li_2S_n (n = 2-8) play a critical role in both for understanding the mechanism of electrode reaction and for improving the performance of lithium-sulfur batteries.[12] However, it is not easy to reveal the details of the reaction

2

mechanism only by experimental methods. For this reason, computational methods were used for investigating the problems arising in the development of lithium-sulfur batteries. Density functional theory (DFT) was used for simulating spectra of lithium polysulfides,[22-25] adsorption processes,[26] and dissolution of lithium polysulfides.[27] Ab initio MD simulations and force filed simulations using ReaxFF were also used for studying reaction processes.[28-34] Thermodynamic stability of lithium polysulfides were studied by DFT calculations.[20,21] Assessment of DFT functionals for lithium-sulfur battery research based on more reliable CCSD(T) calculations was reported.[19] Although these studies have provided valuable information for elucidating the reactions in lithium-sulfur batteries, the detailed mechanism of the Li_2S formation process have not yet been well understood. Especially details of the thermodynamics of Li_2S_n, which are essential for understanding the reduction processes of S_8 to Li_2S, are not clear. Our calculations showed that accurate electron correlation correction is significantly important for studying geometries and energies of S_n. Therefore, we studied the stable structures and thermodynamics of S_n, $S_n^{\cdot-}$, S_n^{2-}, $[LiS_n]^-$ and Li_2S_n (n = 1-8) and discussed the heats of various reduction reactions based on CCSD(T) calculations in this work. The thermodynamics of S_n (n = 1-7) and $S_n^{\cdot-}$ will be useful for understanding the reactions of S_n + 2 Li -> S_{n-1} + Li_2S and the reduction reactions producing radical species, although we do not discuss these reduction reactions in this paper.

Computational methods

The Gaussian 16 program[35] was used for the *ab initio* molecular orbital calculations. The geometries of S_n, $S_n^{\cdot-}$, S_n^{2-}, $[LiS_n]^-$ and Li_2S_n (n = 1-8) were optimized at the MP3/cc-pVDZ level.[36] The energies were calculated at the CCSD(T)/cc-pVTZ level[37] using the optimized geometries. The numbers of initial geometries used for the geometry optimizations, which are summarized in Table 1S, increase by the increase of the number of sulfur atoms. More than one hundred initial geometries were used for the geometry optimizations of S_8, S_8^- and S_8^{2-} to find the most stable structures, respectively. The atomic charge distributions were calculated by electrostatic potential fitting from the MP3/cc-pVTZ level wave functions using the Merz-Singh-Kollman scheme.[38,39] The solvation energies of S_8 and S_n^{2-} (n = 1-8) were calculated using polarizable continuum model[40] at the B3LYP/cc-pVTZ level. The heats of sublimation of Li, S_8 and Li_2S were evaluated from the differences between the calculated energies of crystals and isolated molecules obtained by DFT calculations using B86R exchange functional with the nonlocal correlation functional of vdW-DF2.[41] QUANTUM ESPRESSO[42,43] was used

for the DFT calculations. The cutoff energy in the DFT calculations was 30 Ry (408 eV).

Results and discussion

Optimized structures and relative energies of S_n, $S_n^{\cdot-}$, S_n^{2-}, $[LiS_n]^-$ and Li_2S_n

The geometries for various isomers of S_n (**1-8**), $S_n^{\cdot-}$ (**9-16**), S_n^{2-} (**17-24**), $[LiS_n]^-$ (**25-32**), and Li_2S_n (**33-40**) (n = 1-8) were optimized. The optimized structures and the relative energies of isomers are shown in Figures 1S-34S in supplementary information. The energies calculated for the most stable structures are summarized in Table 1.

Effects of basis set and electron correlation

The basis set and electron correlation correction method used for the calculations of geometries and relative energies were selected based on the analysis of the effects of basis set and electron correlation correction on the calculations of the isomers of S_8. The relative energies calculated for the seven isomers of S_8 (**8a-8g**) at the MP3 level using several basis sets are shown in Figure 35S. The geometries of the isomers of S_8 are shown in Figure 6S. The most stable structure (**8a**) has a ring structure. The basis set effects on the calculated relative energies for the three stable isomers (**8a, 8b** and **8c**) are small, while the basis set effects on the calculated relative energies for other isomers are stronger. Especially the basis set effects on the calculated relative energy for **8g**, which have four parallel S_2s, are very strong. The energies calculated for **8g** relative to **8a** using large basis sets (cc-pVTZ, cc-pVQZ and aug-cc-pVTZ basis sets) are nearly identical, while the other small basis sets underestimate the energy of **8g** relative to **8a**. The relative energies calculated for seven isomers of S_8 at the CCSD(T) level are shown in Figure 36S. The basis set effects observed in the CCSD(T) calculations are similar to those obtained in the MP3 calculations.

The choice of electron correlation correction method has significant impact on the calculated relative energies for the seven isomers of S_8. The relative energies calculated for the seven isomers of S_8 with several electron correlation correction methods using the cc-pVTZ basis set are shown in Figure 37S. The MP2 calculations fail to reproduce the most stable ring structure of **8a**. The MP2 calculations show that the most stable structure **8g** is about 25 kcal/mol more stable than **8a**. The agreement of the calculated relative energies by the MP3 and CCSD methods with those by the CCSD(T) method is much better than the MP2 method. The MP3 and CCSD calculations show that **8a** is the

most stable. These calculations show that higher order electron correlation correction is significantly important for studying stable structures and relative energies of sulfur compounds, and therefore we used the MP3 calculations for the geometry optimizations and the CCSD(T) calculations for the evaluation of the relative energies in this study.

Structures of S_n (n = 1-8)

The optimized geometries of various isomers of sulfur (S_n, n = 3-8) and their relative energies are shown in Figure 1S-6S in supplementary information. S_3 prefers non-linear structure (**3a**), in which the S-S-S angle is 115.9°, as shown in Figure 1S. The linear structure of S_3 (**3b**), which corresponds to a transition state, is 64.2 kcal/mol less stable than **3a**. The most stable structure of S_4 (**4a**) has *eclipse* conformation as shown in Figure 2S.   The S-S-S angle and S-S-S-S torsional angle in **4a** are 105.1° and 0.0°, respectively. The distance between terminal S atoms is only 3.190 Å owing to the small S-S-S angle and the *eclipse* conformation. The distance between terminal S atoms is significantly shorter than the sum of the van der Waals radii. The short S⋯S distance and the preference of the *eclipse* conformation suggest the existence of attraction between terminal S atoms. The calculated HOMO and HOMO-1 orbitals for **4a** are shown in Figure 38S. These orbitals connect the terminal S atoms in **4a**, which suggests the contributions of the orbital-orbital interactions to the attraction. Similarly, the HOMO-1 orbital of S_4^- (**12a**) connects the terminal sulfur atoms as shown in Figure 39S, while the HOMO and HOMO-1 of S_4^{2-} (**20a**) do not connect as shown in Figure 40S. The *trans* conformation of S_4 (**4c**) is 8.5 kcal/mol less stable than **4a**. S_5 prefers a ring structure (**5a**) as shown in Figure 3S. The most stable chain structure of S_5 (**5b**) has *gauche-gauche* conformation, which is 26.2 kcal/mol less stable than **5a**. The *trans-trans* conformation of S_5 (**5c**) is a transition state. S_6 also prefers ring structures (**6a** and **6b**) as shown in Figure 4S. The chair conformation (**6a**) is most stable. Another local energy minimum structure (**6c**), which has three parallel S_2s, is 16.8 kcal/mol less stable than **6a**. The chain structures (**6d** and **6e**) of S_6 are not stable. They are 39.1 and 41.1 kcal/mol less stable than **6a**, respectively. S_7 and S_8 also prefers ring structures (**7a** and **8a**) as shown in Figures 5S and 6S. **8g** has four parallel S_2s, which is 27.8 kcal/mol less stable than the most stable ring structure of S_8 (**8a**). The most stable structures calculated for S_n, (n = 3-8) are summarized in Figure 1. S_n prefers ring structures, if n is 5 or larger. Although the most stable structure of S_4 has chain structure, the terminal S atoms prefer to have short contact.

Structures of $S_n^{\cdot-}$ (n = 1-8)

The optimized geometries of isomers of polysulfide monoanions ($S_n^{\cdot-}$, n = 3-8) and their relative energies are shown in Figure 7S-12S. $S_3^{\cdot-}$ also prefers non-linear structure (**11a**) as in the case of S_3 as shown in Figure 7S. The S-S-S angle in **11a** is 114.7°. The linear structure of $S_3^{\cdot-}$ (**11b**), which corresponds to a transition state, is 57.4 kcal/mol less stable. The most stable structure of $S_4^{\cdot-}$ (**12a**) has *eclipse* conformation as shown in Figure 8S. The S-S-S angle and S-S-S-S torsional angle in **12a** are 107.5° and 0.1°, respectively. The distance between terminal S atoms in $S_4^{\cdot-}$ is only 3.433 Å. Although the distance between terminal S atoms in **12a** is longer than that in **4a** (the most stable structure of S_4), the S⋯S distance is still shorter than the sum of the van der Waals radii. The terminal S atoms of $S_5^{\cdot-}$ have short contact in the most stable structure (**13a**), which has *gauche-gauche'* conformation, as shown in Figure 9S. The distance between terminal S atoms is 3.124 Å. The S⋯S distance in **13a** is significantly shorter than the sum of the van der Waals radii, while it is substantially longer than that of S-S bond. The most stable chain structure of $S_5^{\cdot-}$ (**13b**), which has the *gauche-gauche* conformation, is 1.7 kcal/mol less stable than **13a**. The *trans-gauche* isomer of $S_5^{\cdot-}$ (**13c**) is 1.8 kcal/mol less stable than **13a**. The most stable structure of $S_6^{\cdot-}$ (**14a**) has the *gauche-gauche-gauche'* (*ggg'*) conformation as shown in Figure 10S. The terminal S atoms in the second stable structure of $S_6^{\cdot-}$ (**14b**) have short contact (2.928 Å). **14b** has *gauche-eclipse-gauche'* conformation. The terminal S atoms in the most stable structure of $S_7^{\cdot-}$ (**15a**) and that of $S_8^{\cdot-}$ (**16a**) also have short contacts as shown in Figures 11S and 12S. The distances between terminal S atoms in **15a** and **16a** are 3.011 Å and 2.791 Å, respectively. The most stable structures calculated for $S_n^{\cdot-}$, (n = 3-8) are summarized in Figure 1. The terminal S atoms in $S_n^{\cdot-}$ prefers to have short contact.

Structures of S_n^{2-} (n = 1-8)

The optimized geometries of isomers of polysulfide dianions (S_n^{2-}, n = 3-8) and their relative energies are shown in Figure 13S-18S. S_3^{2-} also prefers non-linear structure (**19a**) as in the cases of S_3 and $S_3^{\cdot-}$ as shown in Figure 13S. The S-S-S angle in **19a** is 115.1°. The linear structure of S_3^{2-} (**19b**), which corresponds to a transition state, is 43.3 kcal/mol less stable. The most stable structure of S_4^{2-} (**20a**) has the *gauche* conformation as shown in Figure 14S. The S-S-S-S dihedral angle in **20a** is 104.6°. The *trans* conformation of S_4^{2-} (**20b**) is 1.6 kcal/mol less stable than **20a**, suggesting that polysulfide dianions prefer *gauche* conformation. Another local energy minimum structure of S_4^{2-} (**20c**), which has two parallel S_2s, is 17.6 kcal/mol less stable than **20a**.

6

The most stable structure of $S_5{}^{2-}$ (**21a**) has the *gauche-gauche* (*gg*) conformation as shown in Figure 15S. The *gauche-gauche'* (*gg'*) conformation of $S_5{}^{2-}$ (**21b**) is 3.0 kcal/mol less stable than **21a**. The most stable structure of $S_6{}^{2-}$ (**22a**) has the *ggg* conformation as shown in Figure 16S. The conformations of $S_6{}^{2-}$ including a reverse direction *gauche* bond (**22b** and **22d**) or a *trans* bond (**22c**) are less stable than **22a**. The most stable structures of $S_7{}^{2-}$ (**23a**) and $S_8{}^{2-}$ (**24a**) have the *gggg* and *ggggg* conformations, respectively, as shown in Figures 17S and 18S. The most stable structures of $S_n{}^{2-}$ (n = 3-8) are shown in Figure 1. The most stable structures of $S_n{}^{2-}$ have the conformation consisting only of *gauche* bonds in the same direction.

The atomic charges calculated for the most stable structures of $S_n{}^{2-}$ (n = 3-8) (Figure 2) show that the negative charges mainly distribute on the terminal S atoms. This suggests that the longer distance between the terminal S atoms is advantageous for the stabilization of $S_n{}^{2-}$. The distance between the terminal S atoms in the *gg* conformation S_5 (**21a**) (6.451 Å) is longer than that in the *gg'* conformation (**21b**) (5.808 Å). The distance between the terminal S atoms in the *ggg* (**22a**), *ggg'* (**22b**), *gg'g* (**22d**) conformation S_6 are 7.856, 7.353 and 6.567 Å, respectively. The *ggg* conformation has the longest distance between terminal S atoms. In addition, the distance between the terminal S atoms in **23a** (the *gggg* conformation S_7) and **24a** (the *ggggg* conformation S_8) are longer than those in other conformations consisting only of *gauche* and *gauche'* bonds. This suggests that the long distance between the terminal S atoms in the conformations consisting only of *gauche* bonds in the same direction is the cause of the stability of these conformations.

Energy of S_n, $S_n{}^{\cdot -}$ and $S_n{}^{2-}$ relative to S_8

Energies of S_n, $S_n{}^{\cdot -}$ and $S_n{}^{2-}$ (n = 1-8) relative to S_8 (**8a**) per one sulfur atom were calculated as summarized in Table 2S. The calculated relative energies are shown in Figure 3. The energy of S_n increases as n decreases. The differences among the calculated energies per one sulfur atom for long S_n chains (n = 3-8) are less than 9 kcal/mol (0.4 eV), while shorter S_ns are significantly unstable. The energies calculated for S_1 and S_2 relative to S_8 are 88.1 and 19.3 kcal/mol (3.82 and 0.84 eV), respectively.

Polysulfide is stabilized by becoming monoanions ($S_n{}^{\cdot -}$, n = 2-8, **10**-**16a**). They are 3.4-7.8 kcal/mol (0.15-0.34 eV) more stable than neutral S_8 (**8a**) per one sulfur atom, while S^- (**9**) is 22.5 kcal/mol (0.98 eV) less stable than S_8. On the other hand,

polysulfide dianions (S_n^{2-}, n = 1-6, **17**-**22a**) are less stable than S_8. Especially S^{2-} (**17**) and S_2^{2-} (**18**) are unstable. They are 166.5 and 51.4 kcal/mol (7.22 and 2.23 eV) less stable than S_8, respectively. The S_7^{2-} (**23a**) and S_8^{2-} (**24a**) are 1.3 and 2.2 kcal/mol (0.06 and 0.10 eV) more stable than S_8, respectively.

Structures of [LiS$_n$]$^-$ (n = 1-8)

The optimized geometries of isomers of [LiS$_n$]$^-$ (n = 1-8) and their relative energies are shown in Figure 19S-26S. The triangle structure [LiS$_2$]$^-$ (**26a**) is 33.2 kcal/mol more stable than the linear structure (**26b**) as shown in Figure 20S. The Li atom has contact with the terminal S atoms in the stable structure of [LiS$_3$]$^-$ (**27a**) as shown in Figure 21S. The Li atom has contact with four S atoms in the stable structure of [LiS$_4$]$^-$ (**28a**) as shown in Figure 22S. The Li atom has contact with four S atoms (the two terminal S atoms and the two S atoms connected to the terminal S atoms) in the stable structure of [LiS$_5$]$^-$ (**29a**) as shown in Figure 23S. The Li atom has contact with four S atoms (the two terminal S atoms and the S atoms connected to the terminal S atoms) in the stable structures of [LiS$_6$]$^-$ (**30a**) and [LiS$_7$]$^-$ (**31a**) as in the case of [LiS$_5$]$^-$ (**29a**) as shown in Figures 24S and 25S. The Li atom has contact with four S atoms (the two terminal S atoms and other two S atoms) in the stable structure of [LiS$_8$]$^-$ (**32a**) as shown in Figure 26S.

The most stable structures of [LiS$_n$]$^-$ (n = 1-8) are shown Figure 4. The Li atom has contact with the terminal S atoms in the most stable structures of [LiS$_n$]$^-$ (n = 2-8). The atomic charges calculated for S_n^{2-} (Figure 2) show that the negative charges are mainly distributed on the terminal S atoms. The strong attractive electrostatic interactions between the Li and the terminal S atoms are apparently the cause of the contact of the Li and the terminal S atoms observed in the most stable structures. Li$^+$ cation has strong electric field owing to the small cation size. The strong electric field and the large atomic polarizability of sulfur atom suggest that the induction interactions (induced polarization) also play important roles in stabilizing the [LiS$_n$]$^-$ complexes.

Structures of Li$_2$S$_n$ (n = 1-8)

The optimized geometries of isomers of Li$_2$S$_n$ (n = 1-8) and their relative energies are shown in Figure 27S-34S. The non-linear Li$_2$S (**33a**) is 0.1 kcal/mol more stable than the linear structure (**33b**) as shown in Figure 27S. The Li-S-Li angle in **33a** is 120.8°. Each Li atom has contact with two S atoms in the stable structure of Li$_2$S$_2$ (**34a**) as

shown in Figure 28S. Each Li atom has contact with three S atoms in the stable structure of Li_2S_3 (**35a**) as shown in Figure 29S. Each Li atom has contact with the terminal S atoms and another S atom in the most stable structures of Li_2S_4 (**36a**) and Li_2S_5 (**37a**) as shown in Figures 30S and 31S. Each Li atom has contact with the terminal S atoms and another S atom in other stable structures of Li_2S_5 (**37c** and **37d**) as in the case of **37a**. **37c** and **37d** are 4.9 and 6.9 kcal/mol less stable than **37a**. Other local minimum structures of Li_2S_5 (**37e**, **37f** and **37g**) are significantly unstable. These structures are 39-59 kcal/mol less stable than **37a**. Each Li atom has contact with the terminal S atoms and another S atom in the most stable structures of Li_2S_6 (**38a**), Li_2S_7 (**39a**) and Li_2S_8 (**40a**) as in the case of Li_2S_5 as shown in Figures 32S-34S. Li_2S_7 and Li_2S_8 have several stable structures. The energies of three stable structures of Li_2S_7 (**39b**-**39d**) relative to **39a** are less than 3 kcal/mol. The energies of four stable structures of Li_2S_8 (**40b**-**40e**) relative to **40a** are less than 4 kcal/mol.

The most stable structures of Li_2S_n (n = 1-8) are shown Figure 5. Each Li atom has contact with the terminal S atoms and another S atom in the most stable structures of Li_2S_n (n = 2-8). The large negative charges on the terminal S atoms are apparently the cause of the contact of each Li and the terminal S atoms observed in the most stable structures. As a result, two Li ions are in contact with each other in the most stable structures of Li_2S_n (n = 4-8). This shows that the stabilization by the attraction between Li^+ and S_n^{2-} overcomes the strong repulsion between Li^+ cations.

Heats of redox reactions of Li_2S_n

The heats of reduction reactions of S_8 and Li_2S_n with Li in the gas phase (ΔE_{gas}) were obtained from the calculated energies of S_8, Li and Li_2S_n summarized in Table 1. The heats of reduction reactions in solid phase (ΔE_{solid}) were estimated using the heats of sublimation (ΔE_{sub}) of S_8, Li and Li_2S shown in Table 2. The details of the estimation procedure of the ΔE_{solid} are shown in supplementary information. The ΔE_{gas} and ΔE_{solid} of 80 reduction reactions, which correspond to discharge reactions, are summarized in Tables 3S-10S. The ΔE_{gas} and ΔE_{solid} of reverse oxidation reactions, which correspond to charge reactions, are summarized in Tables 11S-18S. The ΔE_{gas} and ΔE_{solid} were normalized as one electron reactions. The normalized ΔE_{solid} correspond to the discharge and charge voltage. The reactions were colored according to the magnitude of ΔE_{solid}. The ΔE_{solid} are 0.05 to 0.56 eV greater than the corresponding ΔE_{gas}. The ΔE_{solid} of 80

reduction reactions of S_8 and Li_2S_n (n = 2-8) with Li are in the range of -1.82 to -3.37 eV.

There are a lot of reduction reactions with nearly identical ΔE_{solid} as summarized in Tables 3S-10S, which suggests that several reduction reactions can proceed simultaneously at the same discharge voltage, although the discharging process was often explained by stepwise reduction reactions.

The reduction reaction solely forming Li_2S_2 from S_8 or Li_2S_n with Li are shown in Table 3. The ΔE_{solid} of these four reduction reactions are -2.36 to -2.84 eV. In addition to the four reactions, a large number of reduction reactions can produce Li_2S_2 along with other Li_2S_n. The 40 reduction reactions which can produce Li_2S_2 are summarized in Table 19S. The ΔE_{solid} of these reduction reactions are -2.04 to -3.10 eV, which suggests that Li_2S_2 can generate in a wide discharge voltage range. A large number of reduction reactions can produce Li_2S as in the case of the formation of Li_2S_2. The ΔE_{solid} of the reduction reactions which can produce Li_2S scatter over a wide range (-1.82 to -2.93 eV) as in the case of the reduction reactions producing Li_2S_2, which suggests that Li_2S can also generate in a wide discharge voltage range.

The reduction reactions whose ΔE_{solid} are greater (more negative) than -3.0 eV are summarized in Table 4. These reactions produce Li_2S_n (n = 2-6 and 8) from S_8 or produce Li_2S_n (n = 3-5) from Li_2S_8 or Li_2S_7. The reduction reactions for the formation of Li_2S_n (n = 3-5, 8) from S_8 have large ΔE_{solid} (-3.24 to -3.33 eV). They are significantly greater than the ΔE_{solid} for the direct formation of Li_2S from S_8 with Li (-2.33 eV). The ΔE_{solid} for the formation of Li_2S_7 and Li_2S from S_8 with Li is small (-2.36 eV).

The reduction reactions solely forming Li_2S from S_8 or Li_2S_n (n = 2-8) are summarized in Table 5. Some of these reactions have to occur to complete the reduction of S_8 to Li_2S. The ΔE_{solid} of the reduction reactions solely forming Li_2S from Li_2S_n (n = 2-8) (-1.82 to -2.19 eV) are smaller (less negative) than the ΔE_{solid} of the reduction reactions for the formation of Li_2S_n (n = 2-6 and 8) from S_8 (-3.00 to -3.33 eV) as shown in Figure 6. These results show that the reduction reactions for the formation of Li_2S_n (n = 2-6 and 8) from S_8 can have a higher discharge voltage (more exothermic) than the reduction reactions solely forming Li_2S to complete the reduction of S_8 to Li_2S. The ΔE_{solid} of the

reduction reactions solely forming Li_2S from Li_2S_n (n = 2-8) decrease (becomes less negative) with the decrease of n as shown in Table 5.

The reduction reactions for the formation of Li_2S_n (n = 2-6 and 8) from S_8 is more exothermic than that for the formation of Li_2S directly from S_8, while the reduction reactions for the formation of Li_2S from Li_2S_n are slightly less exothermic than that for the formation of Li_2S directly from S_8. This suggests that a two-step discharge curve, where the reduction reactions for the formation of Li_2S_n (n = 2-6 and 8) from S_8, especially for the formation of Li_2S_n (n = 3-5 and 8), occurs first, followed by the formation of Li_2S from the Li_2S_n (n = 2-6 and 8), is observed, if reactions with large heat generation are favored.

The oxidation reactions for the formation of Li_2S_n (2-8) from Li_2S are slightly less endothermic than that for the formation of S_8 directly from Li_2S, but the oxidation reactions for the formation of S_8 from Li_2S_n (2-8) are much more endothermic compared with that for the formation of S_8 directly from Li_2S. This shows that the oxidation reaction for the formation of S_8 directly from Li_2S can proceed at the lower charge voltage compared with the oxidation reactions for the formation of S_8 from Li_2S_n (n = 3-5, 8).

The solvation will have strong impact on the stability of S_n^{2-}. We have calculated the solvation energies for S_8 and S_n^{2-} (n = 1-8) in sulfolane (E_{solv}) as summarized in Table 20S. The stabilization of S_n^{2-} by the solvation is significant. The calculated E_{solv} for S_n^{2-} (n = 1-8) are -278 to -147 kcal/mol, while the magnitude of E_{solv} for S_8^{2-} is small (-1.4 kcal/mol). The magnitude of E_{solv} for S_n^{2-} decreases, as the number of sulfur atoms increases. Although it is not easy to evaluate the impact of solvation on the energies of reduction reactions accurately, the solvation likely to have strong impact if the dissolution of Li_2S_n occurrs in the discharge process.

Conclusion

The CCSD(T) calculations of S_n, $S_n^{\cdot-}$ and S_n^{2-} (n = 1-8) show that S_n ($5 \leq n$) prefer ring structures and the terminal S atoms often prefer to have close contact in the most stable structures of $S_n^{\cdot-}$ ($4 \leq n$), while S_n^{2-} ($4 \leq n$) prefer chain structures which have the conformations consisting only of *gauche* bonds in the same direction. The atomic

charge distributions calculated for S_n^{2-} show that negative charges mainly distribute on the terminal S atoms. The conformations consisting only of *gauche* bonds in the same direction are advantageous for stabilizing S_n^{2-}, owing to the long distance between the terminal S atoms which have large negative charges. The CCSD(T) calculations of $[LiS_n]^-$ and Li_2S_n (n = 3-8) show that each Li atoms have contact with the terminal S atoms in the most stable structures. As a result, the two Li atoms in the most stable structures of Li_2S_n are close each other. The strong electrostatic interactions of Li^+ with negative charges on the terminal S atoms are apparently the cause of the short contact between the Li and terminal S atoms. The comparison of the energies of S_n, $S_n^{\cdot-}$ and S_n^{2-} (n = 1-8) per one sulfur atom show that S_n^- (n = 2-8) and S_n^{2-} (n = 7, 8) are more stable than S_8. The stability of S_n, $S_n^{\cdot-}$ and S_n^{2-} (n = 1-8) increases by the increase of the number of sulfur atoms. $S^{\cdot-}$ and S^{2-} are significantly less stable compared with $S_n^{\cdot-}$ and S_n^{2-} (n = 2-8).

The estimated ΔE_{solid} of the redox reactions show that several redox reactions can occur with nearly identical ΔE_{solid}, which suggests that several reduction reactions can proceed simultaneously at the same discharge voltage, although the discharging process was often explained by stepwise reduction reactions. The ΔE_{solid} of the reduction reactions producing Li_2S_2 and Li_2S scatter over wide ranges, which suggests the possibility of Li_2S_2 and Li_2S generation in wide discharge voltage ranges. The reduction reactions for the formation of Li_2S_n (n = 2-6 and 8) from S_8 is more exothermic than that for the formation of Li_2S directly from S_8, while the reduction reactions for the formation of Li_2S from the Li_2S_n are slightly less exothermic than that for the formation of Li_2S directly from S_8. This suggests that a two-step discharge curve, where the reduction reactions for the formation of Li_2S_n (n = 2-6 and 8) from S_8 occurs first, followed by the formation of Li_2S from the Li_2S_n (n = 2-6 and 8), is observed, if reactions with large heat generation are advantageous. The oxidation reactions for the formation of Li_2S_n from Li_2S are slightly less endothermic than that for the formation of S_8 directly from Li_2S, but the oxidation reactions for the formation of S_8 from Li_2S_n are much more endothermic compared with than that for the formation of S_8 directly from Li_2S. This suggests that the oxidation reaction for the formation of S_8 directly from Li_2S can proceed at the lower charge voltage compared with the oxidation reactions for the formation of S_8 from Li_2S_n (n = 3-5, 8).

Conflicts of interest

There are no conflicts to declare.

Electronic supplementary information (ESI)

Heats of redox reactions in solid phase, Number of initial geometries used for geometry optimizations of S_n, $S_n^{\cdot-}$, S_n^{2-}, $[LiS_n]^-$ and Li_2S_n, Energies of S_n, $S_n^{\cdot-}$ and S_n^{2-} relative to S_8 per one sulfur atom, Heats of reduction and oxidation reactions of S_8 and Li_2S_n, Optimized geometries of S_n, $S_n^{\cdot-}$, S_n^{2-}, $[LiS_n]^-$ and Li_2S_n, Basis set and electron correlation effects on relative energies of S_8 isomers, Molecular orbitals of S_4, $S_4^{\cdot-}$ and S_4^{2-}.

References

1 R. D. Rauh, K. M. Abraham, G. F. Pearson, J. K. Surprenant, S. B. Brummer, *J. Electrochem. Soc.* **1979**, *126*, 523-527.

2 Y. V. Mikhaylik, J. R. Akridge, *J. Electrochem. Soc.* **2004**, *151*, A1969-A1976.

3 X. Ji, K. T. Lee, L. F. Nazar, *Nat. Mater.* **2009**, *8*, 500-506.

4 P. G. Bruce, S. A. Freunberger, L. J. Hardwick, J.-M. Tarascon, *Nat. Mater.* **2012**, *11*, 19-29.

5 D. Moy, A. Manivannan, S. R. Narayanan, *J. Electrochem. Soc.* **2015**, *162* A1-A7.

6 A. Manthiram, Y. Fu, Y.-S. Su, *Acc. Chem. Res.* **2013**, *46*, 1125–1134.

7 Y.-X. Yin, S. Xin, Y.-G. Guo, L.-J. Wan, *Angew. Chem. Int. Ed.* **2013**, *52*, 13186-13200.

8 A. Manthiram, Y. Fu, S.-H. Chung, C. Zu, Y.-S. Su, *Chem. Rev.* **2014**, *114*, 11751-11787.

9 M. Wild, L. O'Neill, T. Zhang, R. Purkayastha, G. Minton, M. Marinescu, G. J. Offer, *Energy Environ. Sci.* **2015**, *8*, 3477-3494.

10 Z. W. Seh, Y. Sun, Q. Zhang, Y. Cui, *Chem. Soc. Rev.* **2016**, *45*, 5605-5634.

11 X, Shen, H. Liu, X.-B. Cheng, C. Yan, J.-Q. Huang, *Enegy Storage Mat.* **2018**, *12*. 161-175.

12 G. Li, S. Wang, Y. Zhang, M. Li, Z. Chen, J. Lu, *Adv. Mater.* **2018**, *30,* 1705590.

13 M. Cuisinier , P.-E. Cabelguen, B. D. Adams, A. Garsuch, M. Balasubramanian, L. F. Nazar, *Energy Environ. Sci.*, **2014**, *7*, 2697-2705.

14 E. Umeshbabu, B. Zheng, Y. Yang, *Electrochemical Energy Reviews*, **2019**, *2*, 199-230.

15 R. Dominko, R. Demir-Cakan, M. Morcrette, J.-M. Tarascon, *Electrochem. Commun.* **2011**, *13*, 117-120.

16 J. Gao, M. A. Lowe, Y. Kiya, H. D. Abruna, *J. Phys. Chem. C* **2011**, *115*, 25132-25137.

17 C. I. Barchasz, F. Molton, C. Duboc, J.-C. Lepretre, S. Patoux, F. Alloin, *Anal. Chem.* **2012**, *84*, 3973-3980.

18 C.-W. Lee, Q. Pang, S. Ha, L. Cheng, S.-D. Han, K. R. Zavadil, K. G. Gallagher, L. F. Nazar, M. Balasubramanian, *ACS Cent. Sci.* **2017**, *3*, 605-613

19 Q. He, X. Liao, L. Xia, Z. Li, H. Wang, Y. Zhao, D. G. Truhla, *J. Phys. Chem. C* **2019**, *123*, 20737-20747.

20 L. Wang, T. Zhang, S. Yang, F. Cheng, J. Liang, J. Chen, *J. Energy Chem.* **2013**, *22*, 72-77.

21 R. S. Assary, L. A. Curtiss, J. S. Moore, *J. Phys. Chem. C* **2014**, *118*, 11545-11558.

22 M. Hagen, P. Schiffels, M. Hammer, S. Dörfler, J. Tübke, M. J. Hoffmann, H. Althues, S. Kaskel, *J. Electrochem. Soc.* **2013**, *160*, A1205-A1214.

23 T. A. Pascal, K. H. Wujcik, J. Velasco-Velez, C. Wu, A. A. Teran, M. Kapilashrami, J. Cabana, J. Guo, M. Salmeron, N. Balsara, D. Prendergast, *J. Phys. Chem. Lett.* **2014**, *5*, 1547-1551.

24 K. H. Wujcik, T. A. Pascal, C. D. Pemmaraju, D. Devaux, W. C. Stolte, N. P. Balsara, D. Prendergast, *Adv. Energy Mater.* **2015**, *5*, 1500285.

25 Z. Chen, R. Wu, Y. Liu, Y. Ha, Y. Guo, D. Sun, M. Liu, F. Fang, *Adv. Mater.* **2018**, *30*, 1802011.

26 A. D. Dysart, J. C. Burgos, A. Mistry, C.-F. Chen, Z. Liu, C. N. Hong, P. B. Balbuena, P. P. Mukherjee, V. G. Pol, *J. Electrochem. Soc.* **2016**, *163*, A730-A741.

27 M. Vijayakumar, N. Govind, E. Walter, S. D. Burton, A. Shukla, A. Devaraj, J. Xiao, J. Liu, C. Wang, A. Karim, S. Thevuthasan, *Phys.Chem.Chem.Phys.* **2014**, *16*, 10923-10932.

28 B. Wang, S. M. Alhassan, S. T. Pantelides, *Phys. Rev.* **2014**, *2*, 034004.

29 C. Zu, A. Dolocan, P. Xiao, S. Stauffer, G. Henkelman, A. Manthiram, *Adv. Energy Mater.* **2016**, *6*, 150193.

30 E. P. Kamphaus, P. B. Balbuena, *J. Phys. Chem. C* **2017**, *121*, 21105-21117.

31 J. C. Burgos, P. B. Balbuena, J. A. Montoya, *J. Phys. Chem. C* **2017**, *121*, 18369-18377.

32 C. Arneson, Z. D. Wawrzyniakowski. J. T. Postlewaite, Y. Ma, *J. Phys. Chem. C* **2018**, *122*, 8769-8779

33 M. M. Islam, A. Ostadhossein, O. Borodin, A. T. Yeates, W. W. Tipton, R. G. Hennig, N. Kumar, A. C. T. van Duin, *Phys.Chem.Chem.Phys.* **2015**, *17*, 3383-3393.

34 S. P. Beltran, P. B. Balbuena, *ChemSusChem* **2018**, *11*, 1970-1980.

35 Gaussian 16, Revision A.01, M. J. Frisch, G. W. Trucks, H. B. Schlegel, G. E. Scuseria, M. A. Robb, J. R. Cheeseman, G. Scalmani, V. Barone, G. A. Petersson, H. Nakatsuji, X. Li, M. Caricato, A. V. Marenich, J. Bloino, B. G. Janesko, R. Gomperts, B. Mennucci, H. P. Hratchian, J. V. Ortiz, A. F. Izmaylov, J. L. Sonnenberg, D. Williams-Young, F. Ding, F. Lipparini, F. Egidi, J. Goings, B. Peng, A. Petrone, T. Henderson, D. Ranasinghe, V. G. Zakrzewski, J. Gao, N. Rega, G. Zheng, W. Liang, M. Hada, M. Ehara, K. Toyota, R. Fukuda, J. Hasegawa, M. Ishida, T. Nakajima, Y. Honda, O. Kitao, H. Nakai, T. Vreven, K. Throssell, J. A. Montgomery, Jr., J. E. Peralta, F. Ogliaro, M. J. Bearpark, J. J. Heyd, E. N. Brothers, K. N. Kudin, V. N. Staroverov, T. A.

Keith, R. Kobayashi, J. Normand, K. Raghavachari, A. P. Rendell, J. C. Burant, S. S. Iyengar, J. Tomasi, M. Cossi, J. M. Millam, M. Klene, C. Adamo, R. Cammi, J. W. Ochterski, R. L. Martin, K. Morokuma, O. Farkas, J. B. Foresman, and D. J. Fox, Gaussian, Inc., Wallingford CT, 2016.

36 J. A. Pople, J. S. Binkley, R. Seeger, *Int. J. Quantum Chem.* **1976**, *10*, 1-19.

37 J. A. Pople, M. Head-Gordon, and K. Raghavachari, *J. Chem. Phys.* **1987**, *87*, 5968-75.

38 U. C. Singh, P. A. Kollman, *J. Comput. Chem.* **1984,** *5,* 129-145.

39 B. H. Besler, K. M. MerzJr, P. A. Kollman, *J. Comput. Chem.* **1990,** *11,* 431-439.

40 J. Tomasi, B. Mennucci, R. Cammi, *Chem. Rev.* **2005**, *105*, 2999-3093.

41 I. Hamada, *Phys. Rev.* **2014**, *89,* 121103.

42 P. Giannozzi, S. Baroni, N. Bonini, M. Calandra, R. Car, C. Cavazzoni, D. Ceresoli, G. L Chiarotti, M. Cococcioni, I. Dabo, A. Dal Corso, S. de Gironcoli, S. Fabris, G. Fratesi, R. Gebauer, U. Gerstmann, C. Gougoussis, A. Kokalj, M. Lazzeri, L. Martin-Samos, N. Marzari, F. Mauri, R. Mazzarello, S. Paolini, A. Pasquarello, L. Paulatto, C. Sbraccia, S. Scandolo, G. Sclauzero, A. P. Seitsonen, A. Smogunov, P. Umari, R. M. Wentzcovitch, *J.Phys. Condens. Matter* **2009,** *21*, 395502.

43 P. Giannozzi, O. Andreussi, T. Brumme, O. Bunau, M. Buongiorno Nardelli, M. Calandra, R. Car, C. Cavazzoni, D. Ceresoli, M. Cococcioni, N. Colonna, I. Carnimeo, A. Dal Corso, S. de Gironcoli, P. Delugas, R. A. DiStasio Jr., A. Ferretti, A. Floris, G. Fratesi, G. Fugallo1, R. Gebauer, U. Gerstmann, F. Giustino, T. Gorni, J. Jia, M. Kawamura, H.-Y. Ko, A. Kokalj, E. Küçükbenli, M. Lazzeri, M. Marsili, N. Marzari, F. Mauri, N. L. Nguyen, H.-V. Nguyen, A. Otero-de-la-Roza, L. Paulatto, S. Poncé, D. Rocca, R. Sabatini, B. Santra, M. Schlipf, A. P. Seitsonen, A. Smogunov, I. Timrov, T. Thonhauser, P. Umari, N. Vast, X. Wu, S. Baron, *J.Phys. Condens. Matter* **2017**, *29*, 465901.

TABLE 1. Calculated energies for S_n, $S_n{}^{\cdot-}$, $S_n{}^{2-}$, $[LiS_n]^-$, Li and $Li_2S_n{}^a$

n	S_n		$S_n{}^{\cdot-}$		$S_n{}^{2-}$		$[LiS_n]^-$		Li_2S_n	
0									**Li**	-7.4327
1	**1**	-397.6038	**9**	-397.7084	**17**	-397.4789	**25**	-405.2353	**25**	-412.7447
2	**2**	-795.4271	**10**	-795.5022	**18**	-795.3248	**26a**	-803.0276	**26a**	-810.5315
3	**3a**	-1193.1922	**11a**	-1193.2699	**19a**	-1193.1328	**27a**	-1200.8140	**27a**	-1208.3018
4	**4a**	-1590.9367	**12a**	-1591.0127	**20a**	-1590.9192	**28a**	-1598.5836	**28a**	-1606.0647
5	**5a**	-1988.6962	**13a**	-1988.7532	**21a**	-1988.6943	**29a**	-1996.3448	**29a**	-2003.8153
6	**6a**	-2386.4558	**14a**	-2386.4985	**22a**	-2386.4619	**30a**	-2394.0989	**30a**	-2401.5654
7	**7a**	-2784.2004	**15a**	-2784.2520	**23a**	-2784.2240	**21a**	-2791.8514	**21a**	-2799.3101
8	**8a**	-3181.9541	**16a**	-3182.0016	**24a**	-3181.9824	**32a**	-3189.5989	**32a**	-3197.0571

[a] Energies for the most stable geometries calculated at the CCSD(T)/cc-pVTZ//MP3/cc-pVDZ level. Energies are in atomic unit.

TABLE 2. Heats of sublimation of S_8, Li and Li_2S[a]

	ΔE_{sub}
S_8	1.02
Li	1.56
Li_2S	4.23

[a] Heats of sublimation were calculated using a van der Waals density functional. See text. Energies in eV.

TABLE 3. Heats of reduction reactions solely forming Li_2S_2 from S_8 or Li_2S_n with Li[a]

	ΔE_{gas}	ΔE_{solid}
Li + 1/8 S_8 -> 1/2 Li_2S_2	−2.42	−2.84
Li + 1/6 Li_2S_8 -> 2/3 Li_2S_2	−2.14	−2.70
Li + 1/4 Li_2S_6 -> 3/4 Li_2S_2	−2.03	−2.58
Li + 1/2 Li_2S_4 -> Li_2S_2	−1.81	−2.36

[a] Heats of reactions are normalized as one electron reactions. Energies in eV.

TABLE 4. Heats of reduction reactions of S_8 and Li_2S_n with Li^a

	ΔE_{gas}	ΔE_{solid}
Li + 1/2 S_8 -> 1/2 Li_2S_8	−3.23	−3.28
Li + 1/4 S_8 -> 1/4 Li_2S_2 + 1/4 Li_2S_6	−2.80	−3.10
Li + 1/4 S_8 -> 1/4 Li_2S_3 + 1/4 Li_2S_5	−2.94	−3.24
Li + 1/4 S_8 -> 1/2 Li_2S_4	−3.02	−3.33
Li + 1/6 S_8 -> 1/3 Li_2S_2 + 1/6 Li_2S_4	−2.62	−3.00
Li + 1/6 S_8 -> 1/6 Li_2S_2 + 1/3 Li_2S_3	−2.65	−3.04
Li +1/2 Li_2S_8 -> 1/2 Li_2S_3 + 1/2 Li_2S_5	−2.65	−3.20
Li +1/2 Li_2S_8 -> Li_2S_4	−2.82	−3.37
Li + 1/2 Li_2S_7 -> 1/2 Li_2S_3 + 1/2 $Li2S_4$	−2.60	−3.16

[a] Heats of reactions are normalized as one electron reactions. Heats of reactions greater (more negative) than -3.0 eV are shown. Energies in eV.

TABLE 5. Heats of reduction reactions solely forming Li_2S from S_8 or Li_2S_n with Li

	ΔE_{gas}	ΔE_{solid}
Li + 1/16 S_8 –> 1/2 Li_2S	−1.84	−2.33
Li + 1/14 Li_2S_8 –> 4/7 Li_2S	−1.64	−2.19
Li + 1/12 Li_2S_7 –> 7/12 Li_2S	−1.61	−2.17
Li + 1/10 Li_2S_6 –> 3/5 Li_2S	−1.57	−2.12
Li + 1/8 Li_2S_5 –> 5/8 Li_2S	−1.52	−2.08
Li + 1/6 Li_2S_4 –> 2/3 Li_2S	−1.44	−2.00
Li + 1/4 Li_2S_3 –> 3/4 Li_2S	−1.37	−1.93
Li + 1/2 Li_2S_2 –> Li_2S	−1.26	−1.82

[a] Heats of reactions are normalized as one electron reactions. Energies in eV.
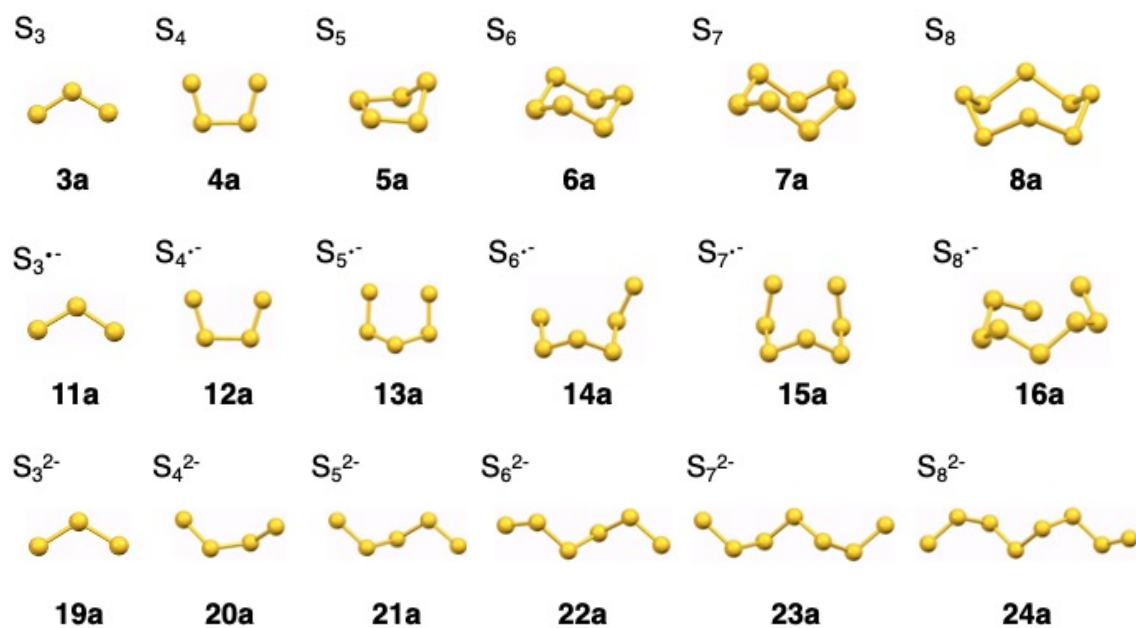
Figure 1 Most stable structures of S_n, $S_n^{\cdot-}$ and S_n^{2-} (n = 3-8).
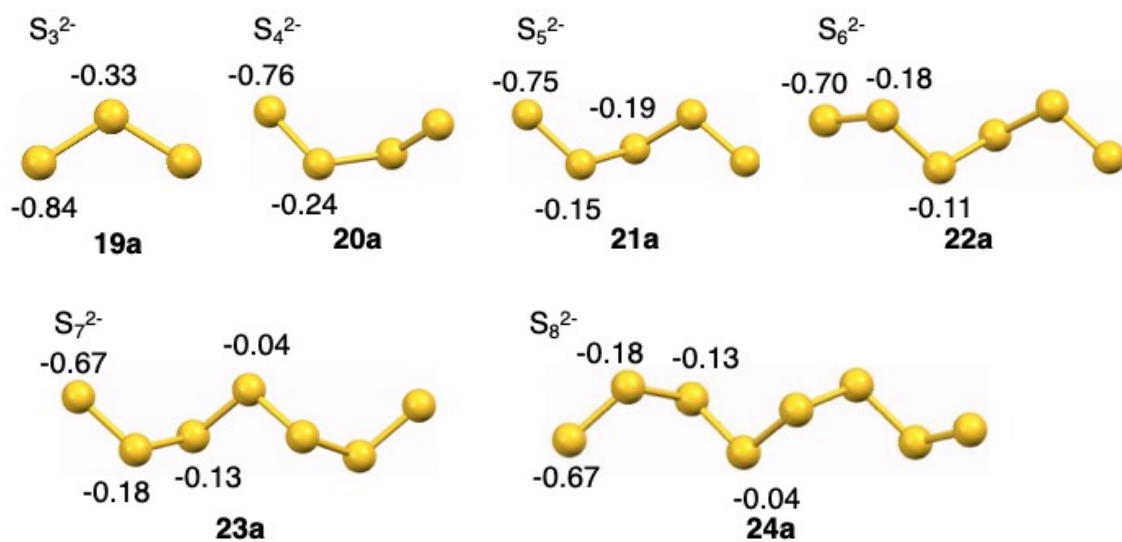
Figure 2.   Partial atomic charges calculated for the most stable structures of S_n^{2-} by electrostatic potential fitting.
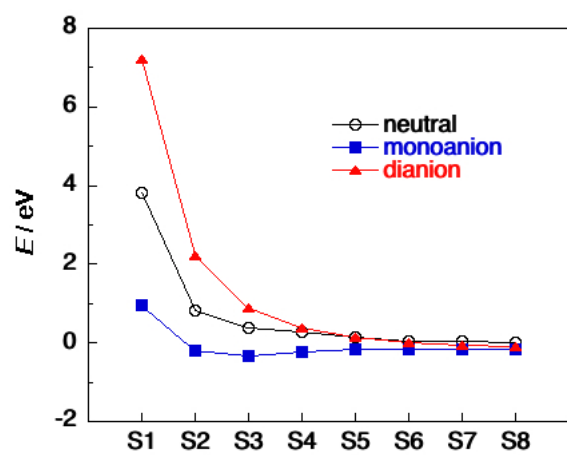
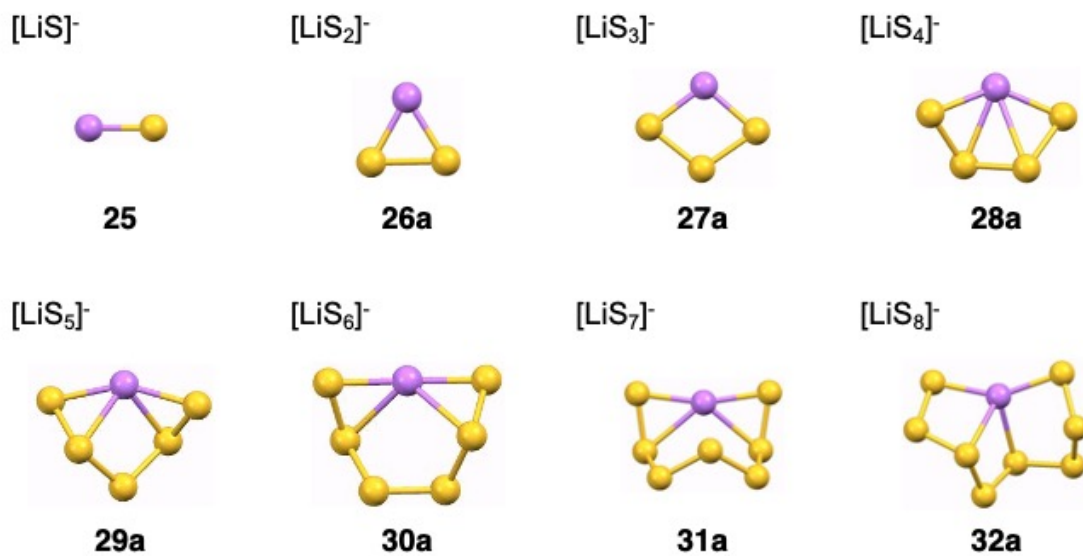Figure 3 Energies of $S_n^{\cdot-}$ and S_n^{2-} (n = 1-8) relative to S_8 per one sulfur atom.

[LiS]⁻

25

[LiS₂]⁻

26a

[LiS₃]⁻

27a

[LiS₄]⁻

28a

[LiS₅]⁻

29a

[LiS₆]⁻

30a

[LiS₇]⁻

31a

[LiS₈]⁻

32a

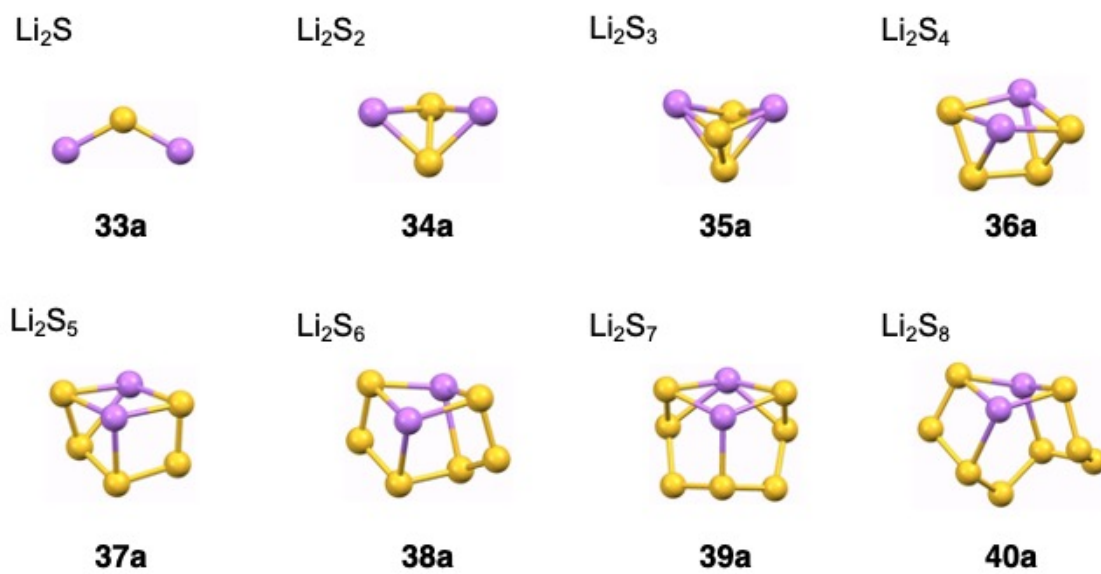Figure 4 Stable structures of [LiS$_n$]⁻ (n = 1-8).

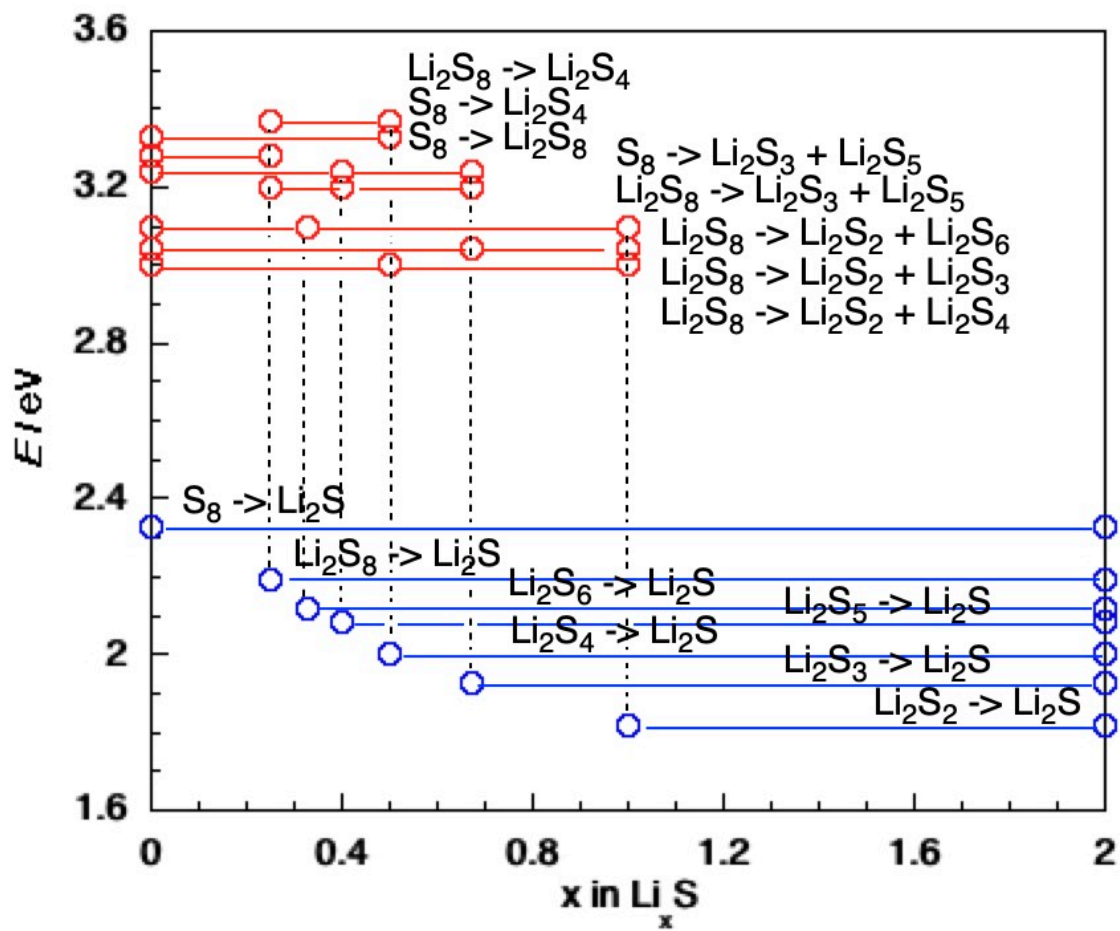Figure 5 Stable structures of Li_2S_n (n = 1-8).

Figure 6 Reduction reactions and their heats of reactions per one electron.